A ceramic electrode of ZrO_2-Y_2O_3 for the generation of oxidant species in anodic oxidation. Assessment of the treatment of Acid Blue 29 dye in sulfate and chloride media

Alexsandro Jhones dos Santos,[a] Sergi Garcia-Segura,[b] Sergi Dosta,[c] Irene García Cano,[c] Carlos A. Martínez-Huitle,[d] Enric Brillas[a,*]

[a] *Laboratori d'Electroquímica dels Materials i del Medi Ambient, Secció de Química Física, Facultat de Química, Universitat de Barcelona, Martí i Franquès 1-11, 08028 Barcelona, Spain*

[b] *Nanosystems Engineering Research Center for Nanotechnology-Enabled Water Treatment, School of Sustainable Engineering and the Built Environment, Arizona State University, Tempe, AZ 85287-3005, USA*

[c] *CPT Thermal Spray Centre, Materials Engineering, Secció de Ciència de Materials, Facultat de Química, Universitat de Barcelona, Martí i Franquès 1-11, 08028 Barcelona, Spain*

[d] *Laboratório de Eletroquímica Ambiental e Aplicada, Instituto de Química, Universidade Federal do Rio Grande do Norte, Lagoa Nova - CEP 59.072-900, Natal, RN, Brazil*Corresponding author: * brillas@ub.edu (E. Brillas)

Abstract

A micron-sized powder of 7% mol Y_2O_3 stabilized ZrO_2 (YSZ) was used to deposit a ceramic coating onto Ti substrate by atmospheric plasma spray. The novel YSZ ceramic presented a dense structure with cubic crystalline structure. The as-synthesized YSZ ceramic as stable anode, coupled to a stainless-steel cathode, was assessed for the anodic oxidation of Acid Blue 29 diazo dye solutions in sulfate and chloride media. The decolorization of these solutions in acidic conditions was clearly faster with chloride as electrolyte, since the generated active chlorine HClO from anodic oxidation of Cl^- was more powerful oxidant than $^\bullet OH$ formed from water discharge at the 7YSZ surface in sulfate medium. In alkaline conditions, the loss of color was drastically reduced because of the conversion of HClO into the weaker oxidant ClO^-, as well as the loss of oxidation power of $^\bullet OH$, partially compensated by the increasing oxidation ability of $SO_4^{\bullet-}$ formed from anodic oxidation of SO_4^{2-} ion. The effect of other experimental variables such as current density, as well as the concentration of each electrolyte and the dye, was examined. The best experimental conditions at pH 7.0 were found for 0.050 M of electrolyte at 20 and 10 mA cm^{-2} using sulfate and chloride media, respectively. In contrast, lower mineralization was achieved in chloride medium because of the formation of very recalcitrant and persistent chloro-derivatives that decelerated the mineralization process. In sulfate medium, NH_4^+, NO_3^- and, to much lesser extent, NO_2^- ions were released during mineralization, whereas tartaric, maleic, acetic and oxalic acids remained in the final solution.

Keywords: Acid Blue 29 dye; Anodic oxidation; Atmospheric plasma spray; Oxidation products; Water treatment; Zirconia-Yttria ceramic

1. Introduction

Anodic oxidation (AO), also called electrochemical oxidation, is one of the most promising electrochemically-driven technologies for the decontamination of waters and wastewaters. In recent years, AO has been largely explored to effectively remove toxic and recalcitrant pollutants including a large variety of pesticides, dyes, drugs and industrial chemicals [1-8]. Emergent electrochemical technologies are considered environmental-friendly since rely on the electron as clean reagent, while addition of hazardous chemicals is not required. AO is classified as an electrochemical advanced oxidation process (EAOP) because electrocatalytically originates *in-situ* adsorbed hydroxyl radical (M($^\bullet$OH)) from water oxidation reaction (1) [1,9,10]. Electrogenerated $^\bullet$OH is a reactive oxygen species (ROS) with a high standard redox potential (E^o) of 2.80 V/SHE.

$$M + H_2O \rightarrow M(^\bullet OH) + H^+ + e^- \tag{1}$$

Even though other ROS such as H_2O_2, $HO_2^\bullet$ and $O_2^{\bullet-}$ can take place concomitantly, the yield of $^\bullet$OH is the most desired for water treatment application. This is explained by the non-selectively attack of $^\bullet$OH to most organic pollutants leading to their overall mineralization towards CO_2 and inorganic ions [1,7,8]. The anode material and electrolyte composition are main variables that determine the oxidation ability of AO over organic pollutants. According to their nature, the anodes can be classified as active and non-active depending on their O_2-overpotential values. Active anodes (e.g., Pt, dimensionally stable anodes) are characterized by a low O_2-overpotential that favors the oxidation of M($^\bullet$OH) to the much weaker oxidant superoxide species MO. These intrinsic characteristics of active anodes promote electrochemical conversion reactions over mineralization events, leading to the conversion of aromatic pollutants into final short-linear carboxylic acids, which are difficultly mineralized to CO_2 [11-14]. In contrast, non-active anodes such as boron-doped diamond (BDD) and PbO_2

3

62 possess much higher O_2-overpotential which stabilize great amounts of physisorbed $M(^\bullet OH)$,

63 allowing the electrochemical incineration of aromatic pollutants [15-20]. The use of PbO_2

64 electrodes arise health concerns due to the leaching risk of lead into water. BDD thin-film

65 electrodes are considered the best anodes for AO. However, the high cost of this advanced

66 carbonaceous material is the main barrier for technology transfer into marked due to the

67 negative impact on expected capital expenses.

68   Ceramic anodes have been extensively used in fuel cells, primordially in solid oxide fuel

69 cells (SOFCs) [21,22]. Good performance has been obtained for complexes composites of

70 $La_{0.75}Sr_{0.25}Cr_{0.5}Mn_{0.5}O_{3-\delta}$-$Ce_{0.9}Gd_{0.1}O_{1.95-\delta}$ and Ni-based materials, like Ni with 8% mol Y_2O_3

71 stabilized ZrO_2 (7YSZ) [23]. These electrodes are cheaper than BDD, highly stable, and present

72 an acceptable electrical resistance. Recently, other ceramics including Ebonex® [24], the

73 substoichiometric TiO_2 in the form of Ti_4O_7 [25-27] and those based on SnO_2-Sb_2O_3 [28-30]

74 have shown an excellent oxidation ability on organic pollutants in waters when used as anodes

75 in AO and related EAOPs (i.e, electro-Fenton (EF)). Table S1 collects some notable results

76 obtained in these works, with a performance usually inferior to that of BDD. Understanding of

77 electrocatalytic oxidation performance of ceramic anodes may open new avenues for

78 electrochemical water treatment technologies competitiveness. Ceramic 7YSZ electrodes must

79 be highlighted as promising anodic materials due to their hardness and chemical inertness,

80 refractivity, and conducting properties. A variety of methods including mechanical milling,

81 reverse microemulsion, hydrothermal, precipitation, sol-gel and thermal decomposition have

82 been utilized for their preparation [31]. The resulting ceramics have been used in jewelry, as

83 non-metallic knife blades, in cements, in electrically-driven processes as electrolyte in SOFC

84 and/or glowing rods in Nernst lamp [23].

85   Water matrix also affects electrochemically driven technologies since it may be a source

86 of additional oxidant species different from $M(^\bullet OH)$. In a classical sulfate medium, the sulfate

87   anion radical ($SO_4^{\bullet-}$) can be formed from the direct anodic oxidation of SO_4^{2-} by reaction (2),

88   which subsequently dimerizes to the weaker persulfate ion ($S_2O_8^{2-}$) by reaction (3) [32,33].

89     $SO_4^{\bullet-}$ is also a very strong oxidant with E^o = 2.5-3.1 V/SHE that reacts via electron-transfer

90   mechanisms, whereas the reaction with M($^\bullet$OH) involves the addition of $-$OH to unsaturated

91   bonds and H-abstraction. The situation is more complex when the medium contains Cl^- ion,

92   because it is oxidized to active chlorine species (Cl_2, HClO and ClO^-) from reactions (4)-(6)

93   [4,28,34-36]. HClO (E^o = 1.49 V|SHE) predominates as oxidant in the pH region 3.0-7.5.

94   Meanwhile, ClO^- with lower oxidation ability (E^o = 0.89 V|SHE) is the stable species at higher

95   pH, according to the acid-base equilibria (pK_a = 7.55). However, active chlorine species can be

96   subsequently transformed into undesirable ClO_2^-, ClO_3^- and ClO_4^- ions, depending on pH and

97   applied current, and can originate toxic and highly recalcitrant chloro-derivatives [4,35].

98     $$SO_4^{2-} \rightarrow SO_4^{\bullet-} + e^- \qquad\qquad (2)$$

99     $$2SO_4^{\bullet-} \rightarrow S_2O_8^{2-} \qquad\qquad (3)$$

100     $$2Cl^- \rightarrow Cl_{2(aq)} + 2e^- \qquad\qquad (4)$$

101     $$Cl_{2(aq)} + H_2O \rightleftarrows HClO + Cl^- + H^+ \qquad\qquad (5)$$

102     $$HClO \rightleftarrows ClO^- + H^+ \qquad pK_a = 7.55 \qquad\qquad (6)$$

103   Textile and food industries consume large amounts of colored dyes, which are partially

104   released in their effluents up to contents of 250 mg L^{-1} [4,37]. These wastewaters can originate

105   serious health risks for living beings because of the toxic, carcinogenic, and mutagenicity

106   characteristics of highly stable organic dyes and their by-products [38,39]. Social awareness of

107   dye pollution concerns is enhanced by aesthetic problems due to the coloration of such effluents

108   [40,41], which propels the need for in situ effluent remediation technologies. However,

109   powerful oxidation techniques are required for the treatment of dyeing effluents since

110   conventional methods such as adsorption and coagulation become very inefficient [38,42].

111   Aromatic azo dyes are the most abundant class of synthetic dyes, which represent about 75%

112   of the overall production of these compounds [43]. They contain one or various -N=N- bonds

113   linked to sulfonic groups to possess a high solubility in water, and they can be efficiently

114   decolorized and mineralized by $^\bullet$OH [44-46]. In this scenario, AO mainly with a BDD or Pt

115   anode has been widely employed for azo dyes removal [4,47-49]. Novel anodes for this

116   technology are needed to be explored to dispose of a high number of materials for practical

117   application.

118   The present paper reports the synthesis of a novel YSZ ceramic onto Ti substrate by

119   atmospheric plasma spray (APS). This is an advanced technique for coatings manufacturing

120   that produces stable deposits from molten particles accelerated onto a substrate. APS reduces

121   electrode manufacturing cost and allows large electrode synthesis in continuous operation. The

122   performance of the synthesized YSZ ceramic as anode in AO was assessed from the treatment

123   of solutions of Acid Blue 29 (AB29) (see molecular structure, name and properties in Table S2)

124   as model diazo dye. The assays were made in sulfate or chloride medium to assess the role of

125   the oxidizing agents produced. The effect of pH, current density (j) and concentration of each

126   electrolyte and of dye over color removal was examined. The chemical oxygen demand (COD)

127   abatement, along with the current mineralization and energetic requirements, were determined

128   in each medium at neutral pH. Finally, the evolution of released nitrogen ions and short-linear

129   carboxylic acids was analyzed to better clarify the mineralization of the dye.

6

2. Materials and methods

2.1. Reagents

Micro-powder fused and crushed powder of 7% mol Y_2O_3 stabilized ZrO_2 (99.9% purity) was supplied by H.C. Starck. Commercial Acid Blue 29 was purchased from Sigma-Aldrich. Analytical grade Na_2SO_4 and NaCl employed as electrolytes were purchased from Sigma-Aldrich. Analytical grade H_2SO_4 (98% purity), HCl (37%) and NaOH supplied by Sigma-Aldrich and Anidrol were used for adjusting the initial solution pH and kept it constant during the experiments. Standard carboxylic acids were purchased from Sigma-Aldrich and Merck. All solutions were prepared with ultrapure Millipore Milli-Q water with resistivity > 18.2 MΩ cm at ambient temperature. Other reagents were either of HPLC or analytical grade supplied by Prolabo, Panreac and Merck.

2.2. Synthesis of the YSZ ceramic onto titanium by APS

The $(ZrO_2)_{0.93}(Y_2O_3)_{0.07}$ micropowder was employed as feedstock to synthesize the YSZ semiconducting ceramic deposit onto titanium by means of APS. This was made with a F4 plasma torch equipped with a Sultzer Metco A-3000S system. This technology involves the heating up, mixing and homogenization of the feedstock microparticles in the hot zone of the plasma jet, followed by their fast acceleration to be quenched onto the substrate producing the coating layer by layer [50-58]. The substrate was a Ti plate (30 mm × 20 mm × 5 mm), previously degreased with acetone and grit blasted with white corundum at 5.6 bar and 45 ºC at 250 mm distance. The average roughness of the resulting substrate was close to 5 μm. The intervals for the spraying parameters of the YSZ coating obtained by APS were: feed rate (10-35 g min^{-1}), spray distance (80-140 mm), applied current (550-650 A), Ar flow plasma (30-45 L min^{-1}) and H_2 flow plasma (8-15 L min^{-1}).

2.3. Electrochemical system

155   All electrolytic experiments were performed with an undivided cylindrical glass tank

156 reactor containing 100 mL of AB29 solution vigorously stirred with a magnetic bar at 600 rpm.

157 The solution temperature was kept at 25 ºC by circulating external thermostated water through

158 a jacket surrounding the cell. The anode was the as synthesized 7YSZ ceramic electrode and

159 the cathode was a stainless steel plate (SS, AISI 304). The geometric area of both electrodes

160 was 6.0 cm^2 and they were placed in parallel at about 1.0 cm. Electrolyses were conducted

161 galvanostatically at *j* values between 5 and 30 mA cm^{-2} using a Minipa MPL-3305 power

162 supply, which directly provided the potential difference between the electrodes. Solutions with

163 AB29 concentration from 10 to 60 mg L^{-1} in two separated electrolytes, Na_2SO_4 or NaCl, with

164 content between 0.025 and 0.100 M at pH 3.0-9.0 were treated by AO.

165 *2.4. Apparatus and analytical procedures*

166   The morphology of the feedstock micro-powder and the as-synthesized ceramic by APS

167 was studied by scanning electron microscopy (SEM) using a JEOL JSM-7100F system. The

168 crystallographic planes of the above materials were determined by X-ray diffraction (XRD)

169 analysis using a Bruker D8 Advance diffractometer, with Cu K_α radiation and a 2θ scan from

170 10° to 110°.

171   The pH of solutions was monitored with a Hanna HI4221 pH-meter. The percentage of

172 color removal of the AB29 solutions treated by AO was calculated by Eq. (7) [4] from the initial

173 absorbance A_0 and the absorbance A at time t measured at $\lambda = 600$ nm, the maximum wavelength

174 of the dye (see Table S2), using an Analytikjena Specord 210 Plus UV/Vis spectrophotometer:

175 % Color removal $= \dfrac{A_0 - A}{A_0}100$ (7)

176   The decolorization kinetics was analyzed from different simple order reaction equations

177 and good linear correlations were found for a pseudo-first-order reaction by plotting $\ln(A_0/A)$

178 vs. t. The COD value of the initial and treated solutions was determined with Hanna instruments

179 COD analytic kits, using a Hanna HI 839800 thermal reactor and a Hanna HI 83099 photometer.

180 From the initial COD_0 and the COD determined at time t (in g O_2 L^{-1}), the percentage of COD

181 removal was obtained from Eq. (8), the percentage of average current efficiency (% ACE) was

182 calculated from Eq. (9) [28] and the electrical energy per order (E_{EO}) was estimated from Eq.

183 (10) [59]:

184 $$\% \text{ COD removal } = \frac{COD_0 - COD}{COD_0} 100 \qquad (8)$$

185 $$\% \text{ ACE } = \frac{F V (COD_0 - COD)}{8 I t} 100 \qquad (9)$$

186 $$E_{EO} \text{ (kWh m}^{-3}\text{)} = \frac{E_{cell} I t}{V \log (COD_0 / COD)} \qquad (10)$$

187 where F is the Faraday constant (96487 C mol^{-1}), V is the solution volume (in L), 8 is the oxygen

188 equivalent mass (in g eq^{-1}), I is the applied current (in A), t is the electrolysis time (in s for %

189 ACE and in h for E_{EO}) and E_{cell} is the average potential difference between electrodes (in V).

190 The produced carboxylic acids were analyzed by high-performance liquid chromatography

191 (HPLC) upon injection of 10 μL aliquots into a Dionex Ultimate 3000 LC via an Ultimate 3000

192 autosampler. The column was an Acclaim Organic Acids (5 μm, 120 Å, 250 mm × 4 mm) and

193 100 mM Na$_2$SO$_4$ at pH 2.6 and 25 ºC was eluted at 600 mL min^{-1} as mobile phase. Carboxylic

194 acids were detected at λ = 210 nm using a Hanna Ultimate 3000 diode array detector, and

195 retention times of 3.7, 4.7, 6.4 and 7.4 min were obtained for oxalic, acetic, maleic and fumaric

196 acids, respectively. Inorganic ions were detected by ion chromatography using a Dionex ICS-

197 3000 LC coupled to a Dionex DS6 conductimetric detector. To do this analysis, 10 μL aliquots

198 were injected through an AS40 autosampler. A Chromeleon CS12A (250 mm × 2 mm) column

199 was used for cation analysis, whereas a Dionex AS19 (250 mm × 2 mm) column was employed

200 for anion determination. Solutions of 20 mM H$_2$SO$_4$ and 50 mM KOH, both at 0.25 mL min^{-1},

201 were used as mobile phases, respectively. Retention times of 4.8 min for NH_4^+ ion, 12.7 min

202 for NO_2^- ion and 16.7 min for NO_3^- ion were found.

203 Average values of the measured % color and % COD removals, released nitrogen inorganic

204 ions and generated carboxylic acids are reported from replicated assays, along with the

205 corresponding error bars with 95% confidence interval in figures.

206 **3. Results and discussion**

207 *3.1. Physical and electrochemical characterization of the as-synthesized 7YSZ ceramic*

208 Fig. 1a and b show SEM images of the commercial YSZ micro-powder. As can be seen,

209 this material was composed of irregular microparticles with a size between 5 and 25 μm. In

210 contrast, the SEM image of Fig. 1c evidences a porous YSZ ceramic coating with the typical

211 lamellar structure of a thermally sprayed coating synthesized from melting and acceleration of

212 the microparticles onto a Ti substrate.

213 Fig. 2 depicts the XRD pattern of the YSZ synthesized ceramic, showing the peaks related

214 to a cubic YSZ from ICS #90885 [31]. The first peaks appeared at 2θ angles of 20.21º (greater

215 intensity), 35.14º, 50.29º, 59.96º, 62.73º and 74.2º corresponding to the (111), (200), (220),

216 (311) and (222) crystallographic planes of its cubic structure, respectively [60].

217 *3.2. Decolorization of Acid Blue 29 in sulfate medium*

218 First studies on the treatment of AB29 solutions by AO using a 7YSZ/SS cell were made

219 by determining their decolorization rate separately in two electrolytes, namely Na_2SO_4 and

220 NaCl. In each medium, the effect of key experimental variables, including the pH, current

221 density and the concentration of electrolyte and diazo dye, was examined. In each assay, the

222 solution pH was continuously regulated to its initial value by adding small volumes of 1 M

223 H_2SO_4, 1 M HCl or 1 M NaOH. Table 1 summarizes the results obtained in all these assays.

224   The solution pH was the first variable examined in sulfate medium because it can determine

225   the role of oxidants M($^\bullet$OH) and SO$_4^{\bullet-}$ [1,4,5,61,62]. Fig. 3a depicts the percentage of color

226   removal vs. time plots for 100 mL of 15 mg L^{-1} dye solutions in 0.050 M Na$_2$SO$_4$ at the pH

227   interval 3.0-9.0 by applying a j = 20 mA cm^{-2} lasting 360 min. A gradual drop in decolorization

228   rate can be observed in the sequence pH 3.0 > pH 5.0 > pH 7.0 > pH 9.0, achieving a final loss

229   of color from 98.9% to 83.7% (see Table 1). This behavior cannot be ascribed to a change in

230   structure of an azo dye with strongly basic lateral sulfonate groups like AB29, because it is

231   expected that its dianionic form (see formula in Table S2) is always the oxidized species in such

232   pH region [4]. The loss of oxidation power with increasing pH can be related to the gradual

233   decreasing production of M($^\bullet$OH) since this radical is more easily oxidized and deactivated by

234   reaction with OH$^-$ to form H$_2$O and O$^-$ [61]. It has been established for other anodes like BDD

235   that SO$_4^{\bullet-}$ generated from reaction (2) possesses much greater oxidation ability in alkaline that

236   in acidic media, even superior to M($^\bullet$OH) [62]. That means that using the 7YSZ ceramic as

237   anode at pH 3.0, the dye removal occurred mainly via the attack of the stronger oxidant M($^\bullet$OH)

238   with low participation of the weaker SO$_4^{\bullet-}$. In contrast, as pH rose to pH 9.0 the dye was less

239   decolorized because M($^\bullet$OH) became less oxidant, not being compensated by the larger action

240   of the more powerful SO$_4^{\bullet-}$.

241   Fig. 3b highlights that the decay of the absorbance associated with the percentage of color

242   removal for the above trials obeyed a pseudo-first-order kinetics. The corresponding apparent

243   rate constant for decolorization (k_{dec}) showed a progressive drop from pH 3.0 to 9.0, varying

244   from 1.29×10^{-2} to 5.0×10^{-3} min^{-1} (see Table 1). The excellent R^2-values obtained ($\geq$ 0.990)

245   validates the kinetic behavior found. This suggests that the decolorization process is controlled

246   by the mass transport of the dye toward the 7YSZ ceramic anion, with a steady production of

247   oxidizing agents at each pH tested [1].

248   The quantity of oxidizing agents produced by the electrolytic system is governed by the

249   applied j. To check the influence of this variable, a solution with 15 mg L^{-1} dye in 0.050 M

250   Na_2SO_4 at pH 7.0 was degraded between 5 and 30 mA cm^{-2}. The neutral pH was selected to

251   mimic the ambient conditions in which dyes can be found. Fig. 4a evidences the enhancement

252   of the percentage of color removal when j grew, up to a maximal from 62.2% at 5 mA cm^{-2} to

253   95.2% at 30 mA cm^{-2}. This is the expected behavior by the concomitant increase in rate of

254   reactions (1) and (2), with generation of greater amounts of oxidants $M(^{\bullet}OH)$ and $SO_4^{\bullet-}$,

255   respectively. However, Fig. 4a reveals that a very similar decolorization was reached operating

256   at 20 and 30 mA cm^{-2}, meaning that the electrolytic system has already attained the maximum

257   oxidation power to destroy the dye and its colored products. This behavior can be accounted by

258   the quicker consumption of the oxidizing agents in waste reactions with detrimental of organic

259   events when the current passed from 20 to 30 mA cm^{-2}. These waste reactions involve, for

260   example, the anodic oxidation of $M(^{\bullet}OH)$ to O_2 gas and the dimerization of $M(^{\bullet}OH)$ to form

261   the weak oxidant H_2O_2 [1,4], as well as the dimerization of $SO_4^{\bullet-}$ to $S_2O_8^{2-}$ via reaction (3).

262   From these results, one can conclude that 20 mA cm^{-2} is the optimum j for dye decolorization

263   in sulfate medium using our electrolytic system. Good pseudo-first-order kinetics with k_{dec}-

264   values raising from 2.8×10^{-3} to 8.3×10^{-3} min^{-1} in the j range of 5-30 mA cm^{-2} were determined

265   for these trials (see Table 1), corroborating the mass-transport control and the formation of

266   steady and small amounts of oxidants in all cases.

267   The study of the influence of Na_2SO_4 concentration between 0.025 and 0.100 M over the

268   loss of color of 15 mg L^{-1} AB29 at pH 7.0 and the optimized j of 20 mA cm^{-2} is presented in

269   Fig. 4b. An upgrading of the percentage of color removal can be observed when the Na_2SO_4

270   content rose from 0.025 to 0.050 M, whereupon no significant change occurred. This can also

271   be deduced from the analogous k_{dec}-values of $(7.7-8.1) \times 10^{-3}$ min^{-1} determined between 0.050

272   and 0.100 M, as shows Table 1. The faster decolorization achieved for 0.050 M Na_2SO_4 as

273   compared to 0.025 M Na_2SO_4 can be attribute to the increase in rate of reaction (2) to generate

274   more quantity of $SO_4^{\bullet-}$. However, the acceleration of the waste reaction (3) for higher

275   electrolyte concentrations impedes more production of oxidant $SO_4^{\bullet-}$, then not affecting the

276   decolorization rate of the dye. This indicates that a content of 0.050 M of Na_2SO_4 is optimal in

277   our experimental conditions.

278   The last experimental variable examined was the dye concentration. Its influence over the

279   decolorization process was studied for contents between 10 and 160 mg L^{-1} in 0.050 M Na_2SO_4

280   at pH 7.0 and $j = 20$ mA cm^{-2}. Fig. 4c evidences that the percentage of color removal underwent

281   a gradual decrease with increasing AB29 concentration. The solution was completely

282   decolorized for 10 mg L^{-1}, but its color was only reduced by 48.3% for 60 mg L^{-1}. This tendency

283   can also be established from the corresponding k_{dec}-values collected in Table 1. The loss of

284   decolorization effectiveness at higher organic load can be ascribed to the smaller proportion of

285   dye removed from the analogous quantity of oxidizing agents produced in all media. Then, the

286   electrolytic system does not lose oxidation ability and only longer time is required to achieve

287   an overall decolorization of the solution.

288   *3.3. Decolorization of Acid Blue 29 in chloride medium*

289   The study of the decolorization of the dye solutions was extended to NaCl as electrolyte

290   for the same interval of experimental variables as taken in Na_2SO_4 medium. However, it was

291   observed that the degradation process was much faster using NaCl and for this reason, the

292   operation time was shortened to 240 min. Fig. 5a shows the change of the percentage of color

293   removal with electrolysis time for 15 mg L^{-1} AB29 solutions in 0.050 M NaCl within the pH

294   region of 3.0-9.0 at $j = 10$ mA cm^{-2}. The decolorization rate was rapidly reduced in the order

295   pH 3.0 >> pH 5.0 > pH 7.0 > pH 9.0. Thus, at pH 3.0 total loss of color was achieved after 120

296   min of electrolysis, but only 54.0% of color was removed at the end of the treatment at pH 9.0.

297   Although the tendency is the same as that of Na_2SO_4 (see Fig. 3a), a much rapid color reduction

13

298 was found in NaCl, at least up to pH 7.0. That can be explained by the action of other strong

299 oxidant such as active chlorine originated from reactions (4)-(6). Much greater amount of active

300 chlorine than M($^{\bullet}$OH) is then expected to be formed at the surface of the 7YSZ ceramic anode.

301 The quickest degradation at pH 3.0 is due to the main oxidation with the most powerful active

302 chlorine, i.e., HClO. When the pH increases, its basic form, i.e., ClO$^-$, is being more produced

303 according to reaction (6) and at pH 9.0 it predominates largely in the medium leading to a

304 slower decolorization because of its smaller oxidation power. Fig, 5b depicts the excellent linear

305 profiles obtained at all pH values by representing the corresponding plots of ln(A_0/A) vs.

306 electrolysis time, thus showing that the decolorization kinetics follows a pseudo-first-order

307 reaction. Table 1 collects the k_{dec}-value, with good R^2 (> 0.97), determined for these

308 experiments, which is as high as 7.45×10^{-2} min^{-1} for pH 3.0, but decays drastically up to 3.4×10^{-3}

309 min^{-1} for pH 9.0. These results inform about the reaction of the dye with a steady content of

310 active species in each medium tested.

311   Fig. 6a shows the decolorization profiles determined for 15 mg L^{-1} dye in 0.050 M NaCl at

312 neutral pH and j values from 5 to 30 mA cm^{-2}. The slow loss of color at j = 5 mA cm^{-2}, attaining

313 48.4% at 240 min, was strongly accelerated at j = 10 mA cm^{-2}, where 89.4% decolorization

314 was reached. This strong effect can be related to the large increase in oxidation rate of Cl$^-$ ion

315 by reaction (4) that originates higher amounts of active chlorine (mainly HClO and ClO$^-$) via

316 reactions (5) and (6), which oxidize more rapidly the dye and its colored products. In contrast,

317 further increase of j causes a progressive slowdown of color removal up to 85.2% at 20 mA

318 cm^{-2} and 72.4% at 30 mA cm^{-2}. This is the result of the loss of active chlorine because its greater

319 production enhances the subsequent conversion of HClO and/or ClO$^-$ into ClO$_2$$^-$, ClO$_3$$^-$ and/or

320 ClO$_4$$^-$ ions via reactions (11)-(13) [35,36]:

321    $ClO^- + H_2O \rightarrow ClO_2^- + 2H^+ + 2e^-$ (11)

322     $ClO_2^- + H_2O \rightarrow ClO_3^- + 2H^+ + 2e^-$ (12)

323     $ClO_3^- + H_2O \rightarrow ClO_4^- + 2H^+ + 2e^-$ (13)

324   The kinetic analysis of the absorbance of the assays of Fig. 6a confirmed that the

325   decolorization process always followed a pseudo-first-order reaction. A look of Table 1 allows

326   inferring that the greatest k_{dec} was 8.6×10^{-2} min^{-1} at the best $j = 10$ mA cm^{-2}, which is 2-fold

327   higher than that obtained in 0.050 M Na_2SO_4. This corroborates the quicker oxidation action of

328   active chorine in chloride medium than $M(^\bullet OH)$ and $SO_4^{\bullet-}$ in sulfate one at pH 7.0.

329   A similar tendency as described above by increasing j was also found when NaCl rose from

330   0.025 to 0.100 M by applying the best $j = 10$ mA cm^{-2}. The data of Fig. 6b, as well as the

331   percentage of color removal and k_{dec}-values listed in Table 1, reveal an enhancement of

332   decolorization by raising NaCl content from 0.025 to 0.050 M, whereupon it underwent a

333   gradual reduction up to 0.100 M. This can be explained again by the upgrading of active

334   chlorine from reactions (4)-(6) up to 0.050 M, followed by a progressive larger acceleration of

335   reactions (11)-(13) that produces the concomitant deceleration of decolorization. A 0.050 M

336   NaCl was then optimal for the treatment of AB29 solutions.

337   The expected decay of the percentage of color removal with increasing dye concentration

338   due to the oxidation with similar amounts of active chlorine is shown in Fig. 6c. As can be seen,

339   the decolorization rate became progressively lower when the AB29 content varied between 10

340   and 60 mg L^{-1} using the best conditions of 0.050 M NaCl and $j = 10$ mA cm^{-2} at neutral pH.

341   The greatest loss of color was of 95.1% obtained for 10 mg L^{-1} dye, with the highest k_{dec}-value

342   of 1.99×10^{-2} min^{-1} (see Table 1). These results indicate that the 7YSZ/SS cell was able to

343   decolorize relatively high contents of the diazo dye, although more time is needed at higher

344   organic load.

345   *3.4. Mineralization of Acid Blue 29 solutions*

346   From the aforementioned findings, the mineralization of 100 mL of 15 mg L^{-1} AB29 by

347   AO with the 7YSZ/SS cell was performed under the optimum conditions determined for the

348   sulfate and chloride media at pH 7.0, lasting the treatments up to 600 min. Fig. 7a shows that

349   the use of 0.050 M Na$_2$SO$_4$ at j = 20 mA cm^{-2} led to 90.4% COD reduction, much superior to

350   67.3% removed in 0.050 M NaCl at j = 10 mA cm^{-2}. These results are opposite to the

351   decolorization behavior of the dye, where the active chlorine formed in NaCl medium had much

352   higher oxidation ability than the oxidants M($^{\bullet}$OH) and SO$_4^{\bullet-}$ produced in Na$_2$SO$_4$ one. The

353   lower mineralization power in NaCl can be accounted for by the formation of high recalcitrant

354   chloro-derivatives [4,35,36], which can be even more toxic than the parent molecule. The

355   accumulation of such largely persistent products in the medium causes a strong deceleration of

356   the mineralization process, as can be seen in Fig. 7a.

357   The ACE values calculated from Eq. (9) for the experiments of Fig. 7a are depicted in Fig.

358   7b. Although lower COD removal was obtained for NaCl, higher ACE values were determined

359   due to the smaller applied j of 10 mA cm^{-2}. Fig. 7b shows an ACE drop from 3.4% at 60 min

360   to 2.1% at 600 min as result of the formation of recalcitrant chloro-derivatives and the loss of

361   organic load [1]. In contrast, a slower decay with electrolysis time can be observed for the

362   smaller ACE values calculated for Na$_2$SO$_4$, which varied between 2.0% at 60 min and 1.3% at

363   600 min, mainly due to the loss of organic matter with generation of less recalcitrant products.

364   These tendencies are reflected in the corresponding E$_{EO}$ values calculated from Eq. (10) and

365   presented in Fig. 7c. Much lower E$_{EO}$ values can be seen using NaCl as electrolyte as compared

366   to Na$_2$SO$_4$ because of the lower applied j (10 mA cm^{-2} vs. 20 mA cm^{-2}) giving rise to a smaller

367   E_{cell} (6.8 V vs. 8.1 V). The final electrical energy per order was 84.1 and 95.6 kWh m^{-3} for such

368   media, respectively.

369

370   *3.5. Evolution of products*

371   It is well-known that the sulfonate group of azo dyes is converted into SO_4^{2-} ion during

372   their mineralization by AO [4,28,44,46]. The fate of the initial N (0.146 mM) contained in 100

373   mL of 15 mg L^{-1} AB29 in 0.050 M Na_2SO_4 at pH 7.0 was followed upon electrolysis in the

374   7YSZ/SS cell at the optimum j = 20 mA cm^{-2}. Fig. 8 shows the time-course of the nitrogen

375   inorganic ions detected, which were progressively accumulated during the treatment. Final

376   concentrations of 0.053 mM of NH_4^+ ion (36.3% of initial N), 0.045 mM of NO_3^- ion (30.8%

377   of initial N) and 0.008 mM of NO_2^- ion (5.5% of initial N) were found. This represents a total

378   of 0.106 mM of N in solution, i.e., 72.6 of initial N, when all *N*-organics are destroyed since

379   COD was reduced by 90.4% (see Fig. 7a). This means that about 27% of the initial N was

380   transformed into volatile *N*-products, like N_2 and N_xO_y, as proposed for other azo dyes

381   [44,46,63].

382   Short-linear aliphatic carboxylic acids such as tartaric, maleic, acetic and oxalic, were

383   identified during the AO treatment of the above solution. Fig. 9 shows the evolution of the

384   concentration of these acids with electrolysis time. The three former acids presented a

385   maximum content, followed by a slow decay due to their oxidation to oxalic acid [4], which

386   was the most persistent product. The final concentrations of such acids were 4.05, 0.35, 1.42

387   and 2.27 mg L^{-1}, respectively, corresponding to a total COD of 4.36 mg O_2 L^{-1}. This represents

388   an 84.8% of the remaining COD solution (5.14 mg O_2 L^{-1}, see Fig. 7a), meaning that the

389   enlargement of the mineralization process of AB29 in sulfate medium by AO is due pre-

390   eminently to the persistence of the carboxylic acids formed, along with other undetected

391   recalcitrant products generated to much lesser proportion.

17

4. Conclusions

A uniform, lamellar and porous novel 7YSZ ceramic, with cubic crystallographic structure has been synthesized onto Ti using APS technology. The oxidation power of the 7YSZ ceramic electrode as anode for AO was assessed from the decolorization of AB29 solutions in sulfate and chloride media coupled to a SS cathode. This process was very fast at pH 3.0, but it was slowed down as pH rose up to 9.0. More rapid loss of color was achieved using NaCl as electrolyte. The main oxidant in sulfate medium at pH 3.0 was M($^\bullet$OH), which lost oxidation power with increasing pH, being partially replaced by the increasing oxidation ability of $SO_4^{\bullet-}$. In chloride medium, the most potent active species HClO was the predominant oxidant at pH 3.0, but at neutral and alkaline pH, it was gradually replaced by the weaker ClO^-. The best experimental variables for decolorization at pH 7.0 were 0.050 M Na_2SO_4 for j = 20 mA cm^{-2} and 0.050 M NaCl for j = 10 mA cm^{-2}. Operating under these conditions, a 15 mg L^{-1} diazo dye solution was more quickly mineralized in sulfate medium, achieving 90.4 % COD reduction, with 1.3% ACE and 95.6 kWh m^{-3} E_{EO}. For this assay, the initial N of AB29 was converted into NH_4^+ and NO_3^- ions and, to much lesser extent, into NO_2^- ion. Tartaric, maleic, acetic and oxalic acids were identified as generated short-linear carboxylic acids, which represented about 85% of the COD remaining in the final solution. The 7YSZ anode was stable upon all experimental conditions tested.

References

[1] M. Panizza, G. Cerisola, Direct and mediated anodic oxidation of organic pollutants, Chem. Rev. 109 (2009) 6541-6569.

[2] L. Feng, E.D. van Hullebusch, M.A. Rodrigo, G. Esposito, M.A. Oturan, Removal of residual anti-inflammatory and analgesic pharmaceuticals from aqueous systems by electrochemical advanced oxidation processes. A review, Chem. Eng. J. 228 (2013) 944-964.

[3] O. Ganzenko, D. Huguenot, E.D. van Hullebusch, G. Esposito, M.A. Oturan, Electrochemical advanced oxidation and biological processes for wastewater treatment: a review of the combined approaches, Environ. Sci. Pollut. Res. Int. 21 (2014) 8493-8524.

[4] E. Brillas, C.A. Martínez-Huitle, Decontamination of wastewaters containing synthetic organic dyes by electrochemical methods. An updated review, Appl. Catal. B: Environ. 166-167 (2015) 603-643.

[5] C.A. Martínez-Huitle, M. Panizza, Electrochemical oxidation of organic pollutants for wastewater treatment, Curr. Opin. Electrochem. 11 (2018) 62-71.

[6] H. Särkkä, A. Bhatnagar, M. Sillanpää, Recent developments of electro-oxidation in water treatment - A review, J. Electroanal. Chem. 754 (2015) 46-56.

[7] F.C. Moreira, R.A.R. Boaventura, E. Brillas, V.J.P. Vilar, Electrochemical advanced oxidation processes: a review on their application to synthetic and real wastewaters. Appl. Catal. B: Environ. 202 (2017) 217-261.

[8] S. Garcia-Segura, J.D. Ocon, M.N. Chong, Electrochemical oxidation remediation of real wastewater effluents - A review, Process Saf. Environ. Protect., 113 (2018) 48-67.

[9] B. Boye, P.A. Michaud, B. Marselli, M.M. Dieng, E. Brillas, C. Comninellis, Anodic oxidation of 4-chlorophenoxyacetic acid on synthetic boron-doped diamond electrodes, New Diamond Frontier Carbon Technol. 12 (2002) 63-72.

440   [10] B. Marselli, J. García-Gomez, P.A. Michaud, M.A. Rodrigo, C. Comninellis,

441   Electrogeneration of hydroxyl radicals on boron-doped diamond electrodes, J.

442   Electrochem. Soc. 150 (2003) D79-D83.

443   [11] E.B. Cavalcanti, S. Garcia-Segura, F. Centellas, E. Brillas, Electrochemical incineration

444   of omeprazole in neutral aqueous medium using a platinum or boron-doped diamond

445   anode: degradation kinetics and oxidation products, Water Res. 47 (2013) 1803-1815.

446   [12] A. El-Ghenymy, R.M. Rodríguez, E. Brillas, N. Oturan, M.A. Oturan, Electro-Fenton

447   degradation of the antibiotic sulfanilamide with Pt/carbon-felt and BDD/carbon-felt cells.

448   Kinetics, reaction intermediates, and toxicity assessment, Environ. Sci. Pollut. Res. 21

449   (2014) 8368-8378.

450   [13] F. Sopaj, M.A.Rodrigo, N. Oturan, F.I.Podvorica, J. Pinson, M.A. Oturan, Influence of

451   the anode materials on the electrochemical oxidation efficiency. Application to oxidative

452   degradation of the pharmaceutical amoxicillin, Chem. Eng. J. 262 (2015) 286-294.

453   [14] H. Zazou, N. Oturan, M.S. Çelebi, M. Hamdani, M.A. Oturan, Cold incineration of 1,2-

454   dichlorobenzene in aqueous solution by electrochemical advanced oxidation using

455   DSA/Carbon felt, Pt/Carbon felt and BDD/Carbon felt cells, Sep. Purif. Technol. 206

456   (2019) 184-193.

457   [15] S. Garcia-Segura, J. Keller, E. Brillas, J. Radjenovic, Removal of organic contaminants

458   from secondary effluent by anodic oxidation with a boron-doped diamond anode as

459   tertiary treatment, J. Hazard. Mater. 283 (2015) 551-557.

460   [16] C. Salazar, N. Contreras, H.D. Mansilla, J. Yáñez, R. Salazar, Electrochemical

461   degradation of the antihypertensive losartan in aqueous medium by electro-oxidation with

462   boron-doped diamond electrode, J. Hazard. Mater. 319 (2016) 84-92.

463 [17] L. Labiadh, A. Barbucci, M.P. Carpanese. A. Gadri, S. Ammar, M. Panizza, Direct and

464 indirect electrochemical oxidation of Indigo Carmine using PbO_2 and $TiRuSnO_2$, J. Solid

465 State Electrochem. 21 (2017) 2167-2175.

466 [18] E.M. Siedlecka, A. Ofiarska, A.F. Borzyszkowska, A. Białk-Bielińska, P. Stepnowski, A.

467 Pieczyńska, Cytostatic drug removal using electrochemical oxidation with BDD

468 electrode: Degradation pathway and toxicity, Water Res. 144 (2018) 235-245.

469 [19] A.H. Henke, T.P. Saunders, J.A. Pedersen, R.J. Hamers, Enhancing electrochemical

470 efficiency of hydroxyl radical formation on diamond electrodes by functionalization with

471 hydrophobic monolayers, Langmuir 35 (2019) 2153-2163.

472 [20] X. Sui, X. Duan, F. Xu, L. Chang, Fabrication of three-dimensional networked PbO_2

473 anode for electrochemical oxidation of organic pollutants in aqueous solution, J. Taiwan

474 Inst. Chem. Eng. (2019). DOI: https://doi.org/10.1016/j.jtice.2019.04.007

475 [21] N.K. Monteiro, S.D. Nóbrega, F.C. Fonseca, Ceramic oxide anode with precipitated

476 catalytic nanoparticles for ethanol fueled SOFC, ECS Trans. 35 (2011) 1601-1609.

477 [22] Z. Yang, Z. Pang, T. Zhu, Z. Zheng, M. Han, Fabrication and performance of ceramic

478 anode-supported Solid Oxide Fuel cells, ECS Trans. 57 (2013) 549-554.

479 [23] J. Kim, D. Shin, J.-W. Son, J.-H. Lee, B.-K. Kim, H.-J. Je, H.-W. Lee, K.J. Yoon,

480 Fabrication and characterization of all-ceramic solid oxide fuel cells based on composite

481 oxide anode, J. Power Sources 241 (2013) 440-448.

482 [24] D. Bejan, J.D. Malcolm, L. Morrison, N.J. Bunce, Mechanistic investigation of the

483 conductive ceramic Ebonex® as an anode material, Electrochim. Acta 54 (2009) 5548-

484 5556.

485 [25] A.M. Zaky, B.P. Chaplin, Porous substoichiometric TiO_2 anodes as reactive

486 electrochemical membranes for water treatment, Environ. Sci. Technol. 47 (2013) 6554-

487 6563.

488   [26] S.O. Ganiyu, N. Oturan, S. Raffy, M. Cretin, R. Esmilaire, E.V. Hullebusch, G. Esposito,

489   M.A. Oturan, Sub-stoichiometric titanium oxide (Ti_4O_7) as a suitable ceramic anode for

490   electrooxidation of organic pollutants: A case study of kinetics, mineralization and

491   toxicity assessment of amoxicillin, Water Res. 106 (2016) 171-182.

492   [27] N. Oturan, S.O. Ganiyu, S. Raffy, M.A. Oturan, Sub-stoichiometric titanium oxide as a

493   new anode material for electro-Fenton process: Application to electrocatalytic destruction

494   of antibiotic amoxicillin, Appl. Catal. B: Environ. 217 (1017) 214-223.

495   [28] E. do Vale-Júnior, S. Dosta, I.G. Cano, J.P. Guilemany, S. Garcia-Segura, C.A. Martínez-

496   Huitle, Acid Blue 29 decolorization and mineralization by anodic oxidation with a cold

497   gas spray synthesized Sn-Cu-Sb alloy anode, Chemosphere 148 (2016) 47-54.

498   [29] J. Mora-Gomes, E. Ortega, S. Mestre, V. Pérez-Herranz, M. García-Gabaldón,

499   Electrochemical degradation of norfloxacin using BDD and new Sb-doped SnO_2 ceramic

500   anodes in an electrochemical reactor in the presence and absence of a cation-exchange

501   membrane, Sep. Purif. Technol. 208 (2019) 68-75.

502   [30] M.J. Sánchez-Rivera, J.J. Giner-Sanz, V. Pérez-Herranz, S. Mestre, CuO improved

503          $(Sn,Sb)O_2$ ceramic anodes for electrochemical advanced oxidation processes, Int. J. Appl.

504   Ceram. Technol. 16 (2019) 1274-1285.

505   [31] K. Apriany, I. Permadani, D.G. Syarif, S. Soepriyanto, F. Rahmawati, Electrical

506   conductivity of zirconia and yttrium-doped zirconia from Indonesian local zircon as

507   prospective material for fuel cells, IOP Conf. Ser.: Mater. Sci. Eng. 107 (2016) 012023

508   [32] A. Farhat, J. Keller, S. Tait, J. Radjenovic, Removal of persistent organic contaminants

509   by electrochemically activated sulfate, Environ. Sci. Technol. 49 (2015) 14326−14333.

510   [33] J. Cai, T. Niu, P. Shi, G. Zhao, Boron-doped diamond for hydroxyl radical and sulfate

511   radical anion electrogeneration, transformation, and voltage-free sustainable oxidation,

512   Small (2019) 1900153 (9 pages).

513   [34] A. Anglada, R. Ibañez, A. Urtiaga, I. Ortiz, Electrochemical oxidation of saline industrial
514   wastewaters using boron-doped anodes, Catal. Today 151 (2010) 178-184.

515   [35] V.S. Antonin, M.C. Santos, S. Garcia-Segura, E. Brillas, Electrochemical incineration of
516   the antibiotic ciprofloxacin in sulfate medium and synthetic urine matrix, Water Res. 83
517   (2015) 31-41.

518   [36] E. Mostafa, P. Reinsberg, S. Garcia-Segura, H. Baltruschat, Chlorine species evolution
519   during electrochlorination on boron-doped diamond anodes: *in-situ* electrogeneration of
520   Cl_2, Cl_2O and ClO_2. Electrochim. Acta 281 (2018) 831-840.

521   [37] M. Solís, A. Solís, H.I. Pérez, N. Manjarrez, M. Flores, Microbial decolouration of azo
522   dyes: a review, Process Biochem. 47 (2012) 1723-1748.

523   [38] K.P. Sharma, S. Sharma, S.P. Sharma, K. Singh, S. Kumar, R. Grover, P.K. Sharma, A
524   comparative study on characterization of textile wastewaters (untreated and treated)
525   toxicity by chemical and biological tests, Chemosphere 69 (2007) 48-54.

526   [39] S.M.A.G. Ulson de Souza, E. Forgiarini, A.A. Ulson de Souza, Toxicity of textile dyes
527   and their degradation by the enzyme horseradish peroxidase (HRP), J. Hazard. Mater. 147
528   (2007) 1073-1078.

529   [40] UNESCO, The United Nations World Water Development Report 4, Volume 1:
530   Managing Water Report under Uncertainty and Risk, 2012.

531   [41] A.K. Verma, R.R. Dash, P. Bhunia, A review on chemical coagulation/flocculation
532   technologies for removal of colour from textile wastewaters, J. Environ. Manage. 93
533   (2012) 154-168.

534   [42] A.B. dos Santos, F.J. Cervantes, J.B. van Lier, Review paper on current technologies for
535   decolourisation of textile wastewaters: perspectives for anaerobic biotechnology,
536   Bioresour. Technol. 98 (2007) 2369-2385.

537   [43] D. Rajkumar, J.G. Kim, Oxidation of various reactive dyes with in situ electrogenerated

538   active chlorine for textile dyeing industry wastewater treatment, J. Hazard. Mater. B136

539   (2006) 203-212.

540   [44] S. Garcia-Segura, F. Centellas, C. Arias, J.A. Garrido, R.M. Rodríguez, P.L. Cabot, E.

541   Brillas, Comparative decolorization of monoazo, diazo and triazo dyes by electro-Fenton

542   process, Electrochim. Acta 58 (2011) 303-311.

543   [45] R. Salazar, S. Garcia-Segura, M.S. Ureta-Zañartu, E. Brillas, Degradation of disperse azo

544   dyes from waters by solar photoelectro-Fenton, Electrochim. Acta 56 (2011) 6371-6379.

545   [46] A.M.S. Solano, S. Garcia-Segura, C.A. Martínez-Huitle, E. Brillas, Degradation of acidic

546   aqueous solutions of the diazo dye Congo Red by photo-assisted electrochemical

547   processes based on Fenton's reaction chemistry, Appl. Catal. B: Environ. 168-169 (2015)

548   559-571.

549   [47] V. Santos, A. Morão, M.J. Pacheco, L. Ciríaco, A. Lopes, Electrochemical degradation

550   of azo dyes on BDD: effect of chemical structure and operating conditions on the

551   combustion efficiency, J. Environ. Eng. Manage. 18 (2008) 193-204.

552   [48] X. Florenza, A.M. Sales Solano, F. Centellas, C.A. Martínez-Huitle, E. Brillas, S. Garcia-

553   Segura, Degradation of the azo dye Acd Red 1 by anodic oxidation and

554   indirectelectrochemical processes based on Fenton's reaction chemistry. Relationship

555   between decolorization, mineralization and products, Electrochim. Acta 142 (2014) 276-

556   288.

557   [49] C.N. Brito, M.B. Ferreira, S.M.L. de O. Marcionilio, E.C,M. de M. Santos, J.J.L. Léon,

558   S.O. Ganiyu, C.A. Martínez-Huitle, Electrochemical oxidation of Acid Violet 7 dye by

559   using Si/BDD and Nb/BDD electrodes, J. Electrochem. Soc. 165 (2018) E250-E255.

560   [50] I.G.Cano, S. Dosta, J.R. Miguel, J.M. Guilemany, Production and characterisation of

561   metastable Al_2O_3-TiO_2 ceramic materials, J. Mater. Sci. 42 (2007) 9331- 9335.

562 [51] I.G. Cano, S. Dosta, J.R. Miguel, J.M. Guilemany, Production and characterization of

563   metastable ZrO_2 -Al_2O_3 coatings obtained by APS+ Quench, J. Therm. Spray Technol.

564   17 (2008) 360-364.

565 [52] J. Suffner, H. Sieger, H. Hahn, S. Dosta, I.G. Cano, J.M. Guilemany, P. Klimczyk, L.

566   Jaworska, Microstructure and mechanical properties of near eutectic ZrO_2 - 60 wt.% Al_2O_3

567   produced by quenched plasma spraying, Mater. Sci. Eng. A 506 (2009) 180-186.

568 [53] J. Suffner, H. Hahn, S. Dosta, I.G. Cano, J.M. Guilemany, Influence of liquid nitrogen

569   quenching on the evolution of metastable phases during plasma spraying of (ZrO_2 - 5wt.%

570   Y_2O_3) - 20 wt.% Al_2O_3 coatings, Surf. Coat. Technology 204 (2009) 149-156.

571 [54] J. Suffner, M. Latteman, H. Hahn, L. Giebeler, C. Hess, I.G. Cano, S. Dosta, J.M.

572   Guilemany, C. Musa, A.M. Locci, R. Licheri, R. Orrú, G. Cao, Microstructure evolution

573   during spark plasma sintering of metastable (ZrO_2 - 5wt.% Y_2O_3) - 20 wt.% Al_2O_3

574   composite powders. J. Am. Ceram. Soc. 93 (2010) 2864-2870.

575 [55] S. Dosta, M. Torrell, I.G. Can, J.M. Guilemany, Functional coloured ceramic coatings

576   obtained by thermal spray for decorative applications. J. Eur. Ceram. Soc. 32(2012) 3685-

577   3692.

578 [56] V. Crespo, I.G. Cano, S. Dosta. J.M. Guilemany, Influence of nanostructured ZrO_2

579   additions on the wear resistance of Ni-based alloy coatings deposited by APS process,

580   Wear 303 (2013) 591-601.

581 [57] S. Dosta, M. Robotti, S. Garcia-Segura, E. Brillas, I.G. Cano, J.M. Guilemany, Influence

582   of atmospheric plasma spraying on the solar photoelectro-catalytic properties of TiO_2

583   coatings, Appl. Catal. B: Environ. 189 (2016) 151-159.

584 [58] C.R.C. Lima, S. Dosta, J.M. Guilemany, D.R. Clarke, The application of

585   photoluminescence piezospectroscopy for residual stresses measurement in thermally

586   sprayed TBCs, Surf. Coat.Technol. 318 (2017) 147-156.

587   [59] S. Garcia-Segura, M. Lanzarini-Lopes, K. Hristovski, P. Westerhoff, Electrocatalytic

588   reduction of nitrate: fundamentals to full-scale water treatment applications, Appl. Catal.

589   B: Environ. 236 (2018) 546-568.

590   [60] A. Gupta, S. Sharma, N. Mahato, A. Simpson, S. Omar, K. Balani, Mechanical properties

591   of spark plasma sintered ceria reinforced 8 mol% yttria-stabilized zirconia electrolyte,

592   Nanomater. Energy 1 (2012) 306-315.

593   [61] Q. Zhang, W. Huang, J. M. Hong, B. Y. Chen, Deciphering acetaminophen electrical

594   catalytic degradation using single-form S doped graphene/Pt/TiO_2, Chem. Eng. J. 343

595   (2018) 662-675.

596   [62] L. Chen, C. Lei, Z. Li, B. Yang, X. Zhang, L. Lei, Electrochemical activation of sulfate

597   by BDD anode in basic medium for efficient removal of organic pollutants, Chemosphere

598   210 (2018) 516-523.

599   [63] S. Garcia-Segura, E. Mostafa, H. Baltrushcat, Could NOx be released during

600   mineralization of pollutants containing nitrogen by hydroxyl radical? Ascertaining the

601   release of N-volatile species, Appl. Catal. B: Environ. 207 (2017) 376-384.

602
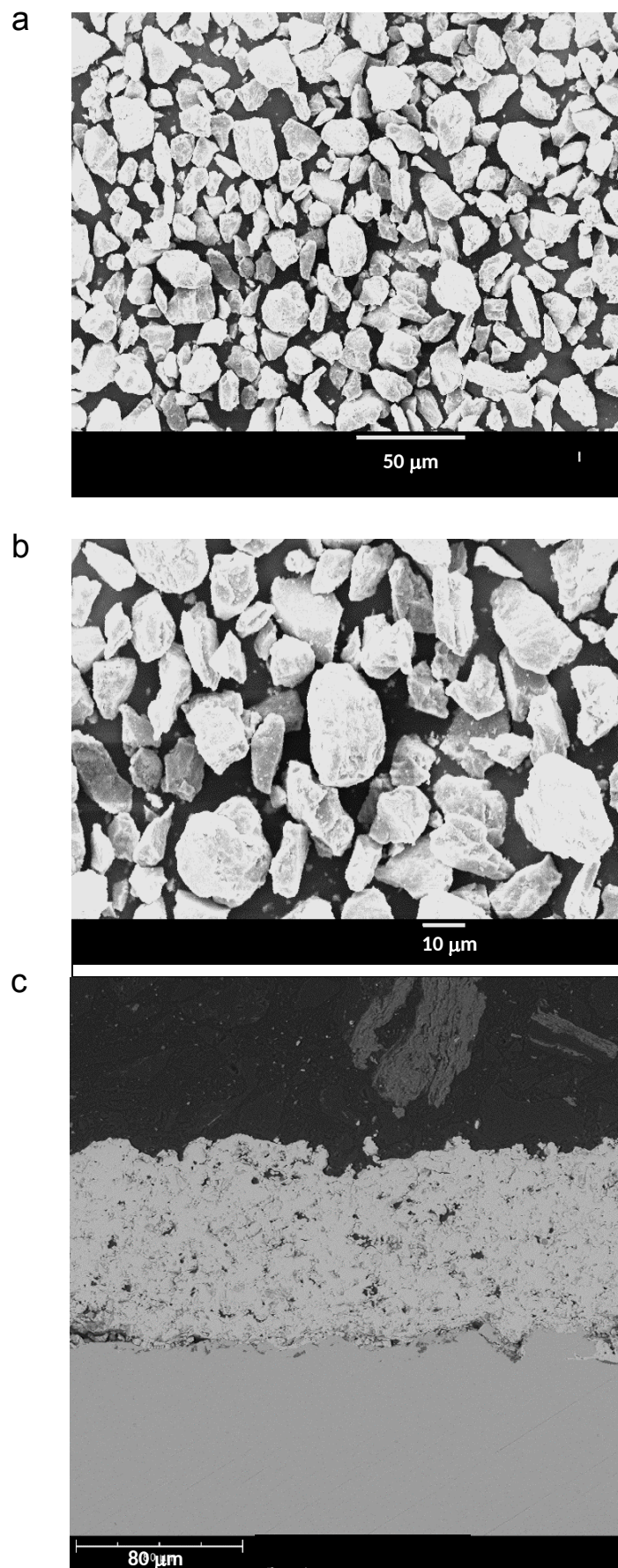
Fig. 1. SEM image of powder at (a) 500X, (b) 1000X and (c) of the as-synthesized 7% mol Y_2O_3 stabilized ZrO_2 (7YSZ) ceramic by atmospheric plasma spray (1000X).
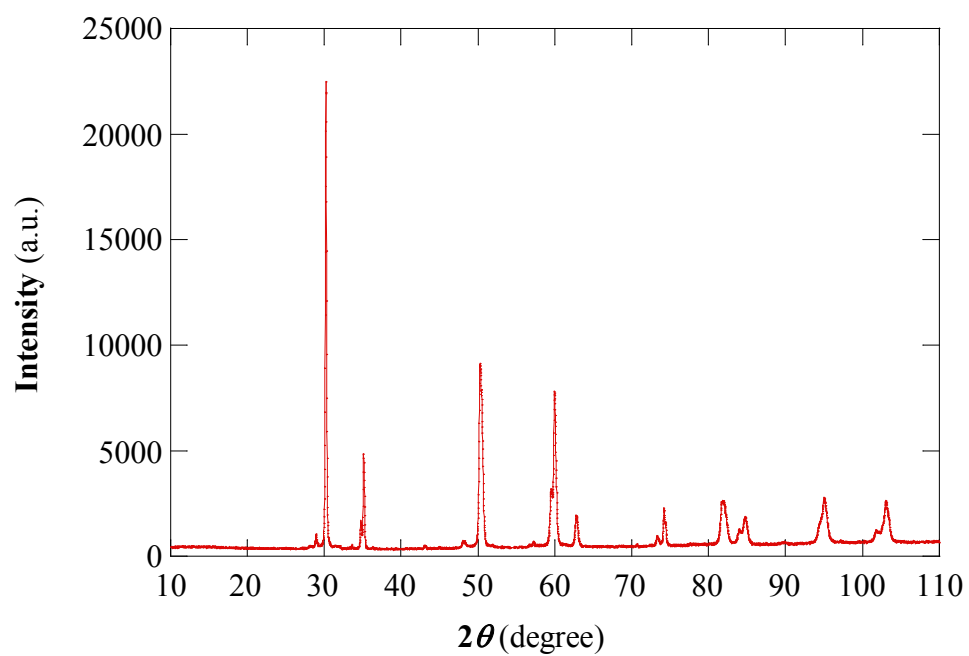
Fig. 2. XRD pattern of the as-synthesized 7YSZ ceramic electrode by atmospheric plasma spray.
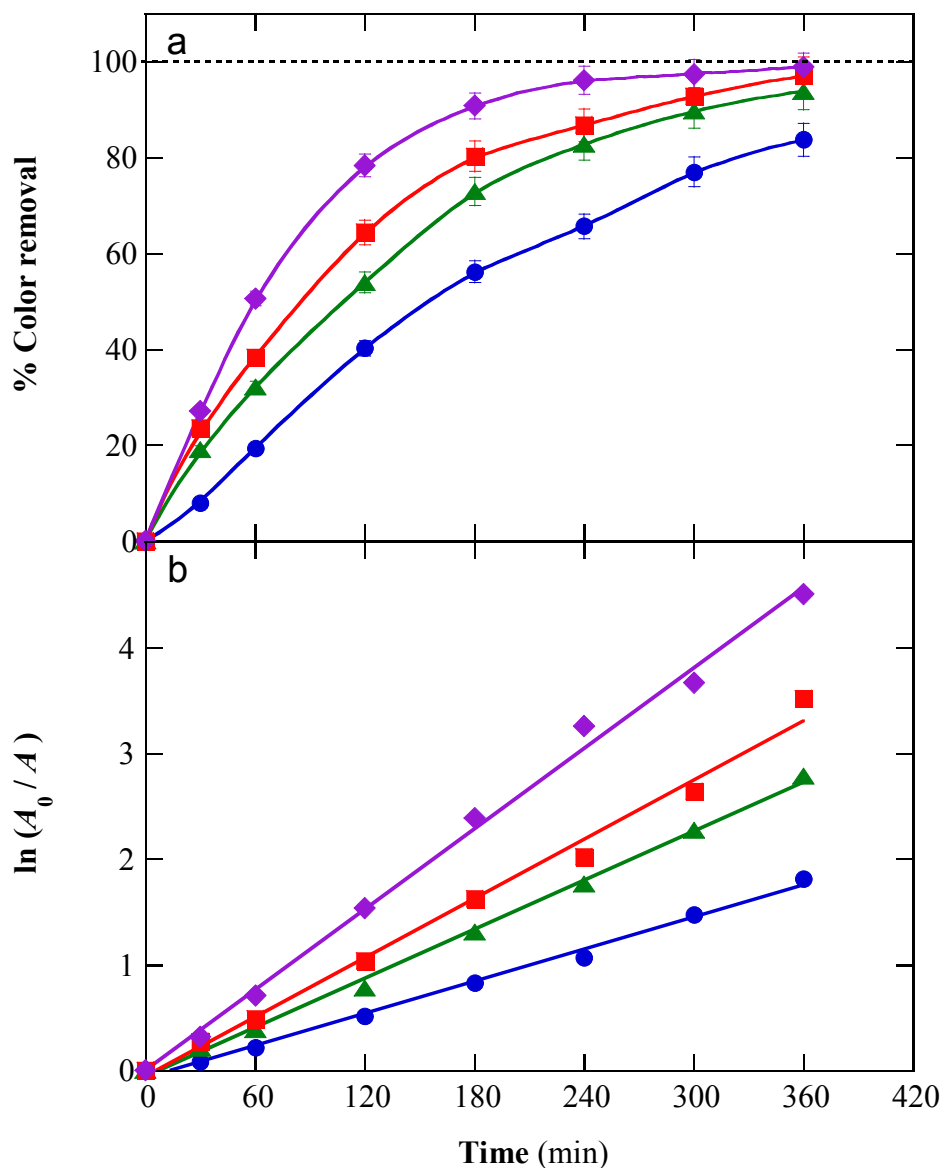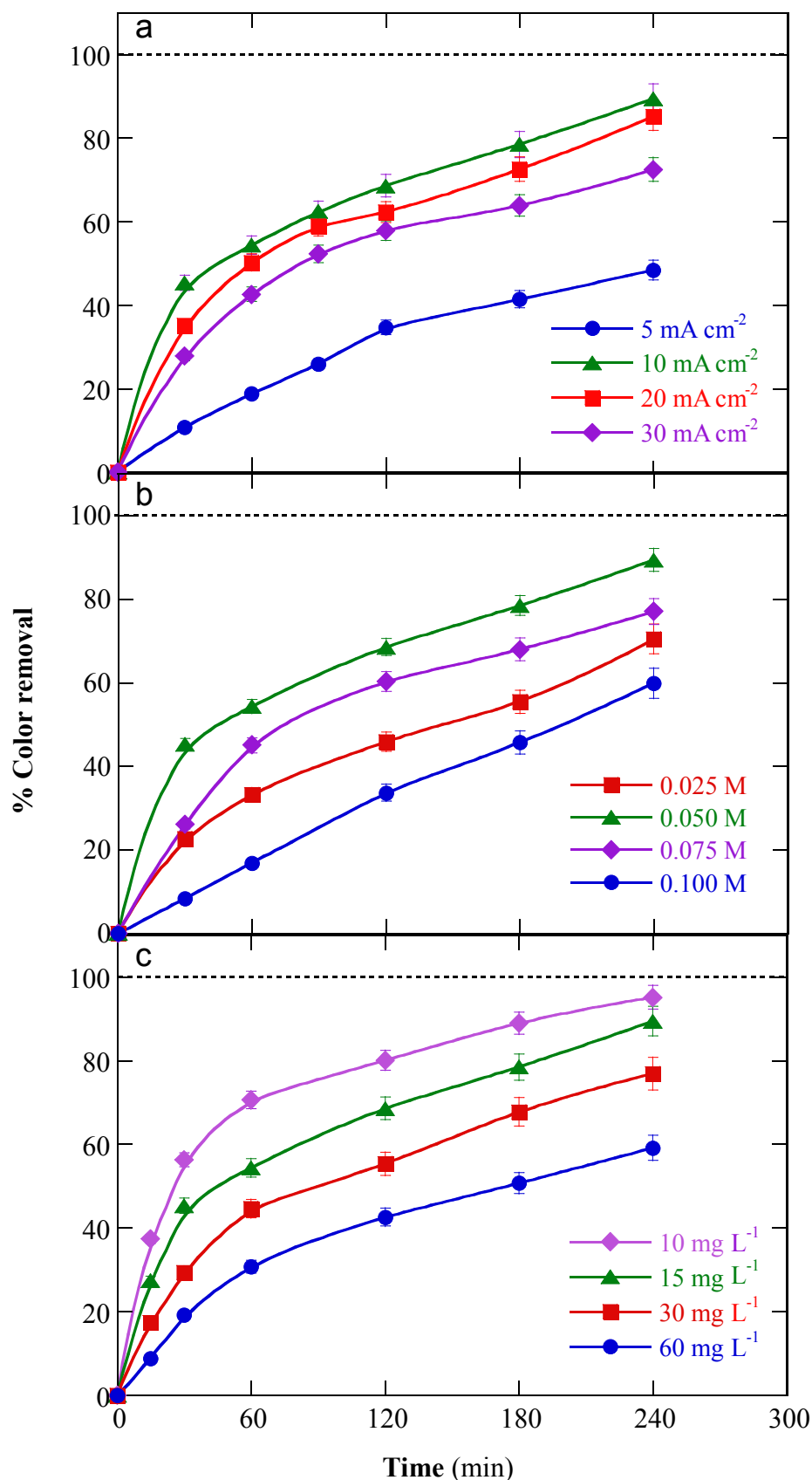
Fig. 3. Effect of pH over (a) percentage of color removal vs. electrolysis time and (b) pseudo-first-order kinetics of the absorbance decay for the anodic oxidation (AO) treatment of 100 mL of 15 mg L^{-1} AB29 in 0.050 M Na$_2$SO$_4$ using a 7YSZ/stainless steel (SS) cell at 20 mA cm^{-2} and 25 °C. Solution pH: (◆) 3.0, (■) 5.0, (▲) 7.0 and (●) 9.0.
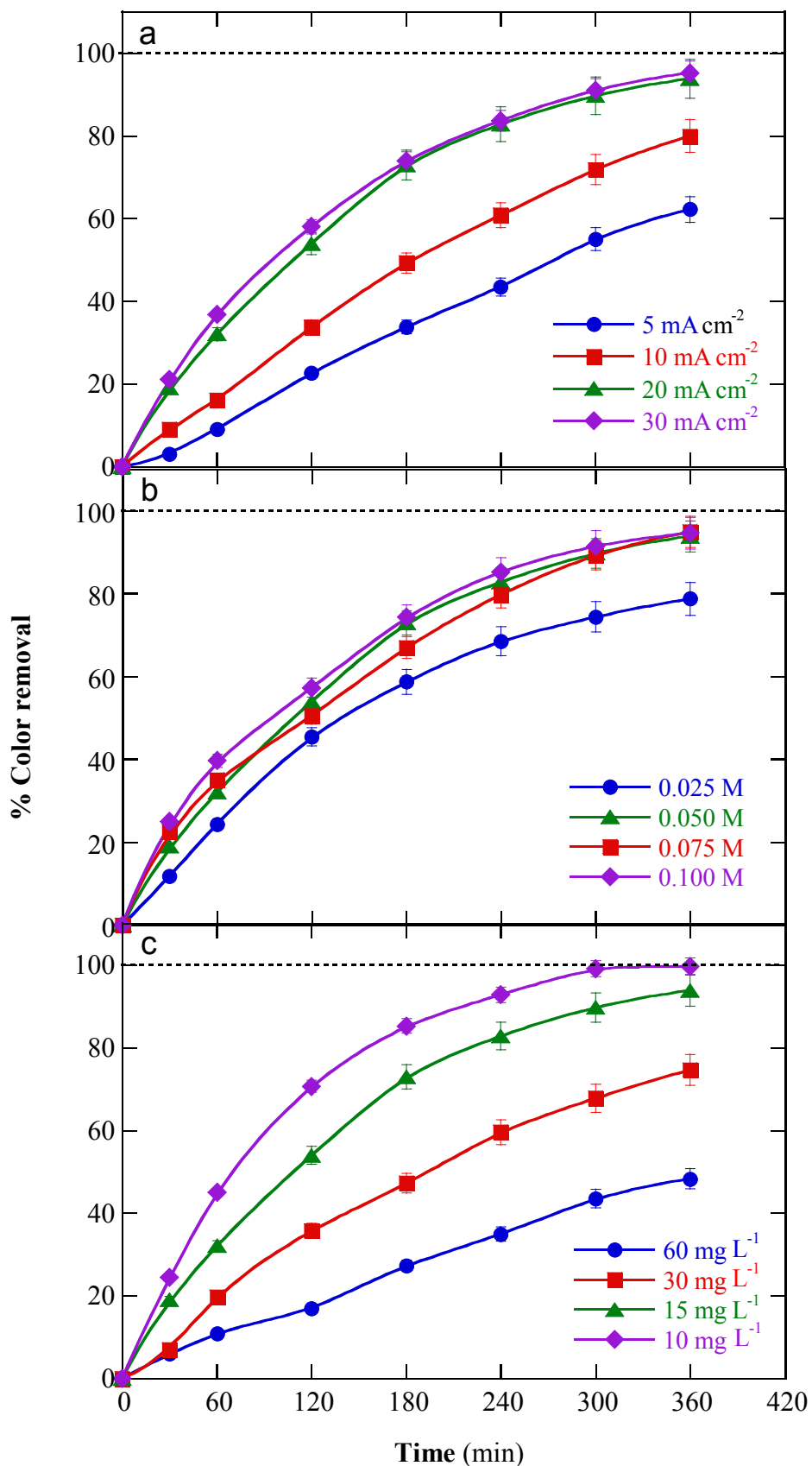
Fig.4. Change of the percentage of color removal with electrolysis time for the AO process of 100 mL of AB29 solutions at pH 7.0 and 25 ºC with a 7YSZ/SS cell. (a) Effect of current density for 15 mg L^{-1} dye in 0.050 M Na_2SO_4. (b) Effect of Na_2SO_4 concentration for 15 mg L^{-1} dye at 20 mA cm^{-2}. (c) Effect of AB29 concentration for 0.050 M Na_2SO_4 and 20 mA cm^{-2}.
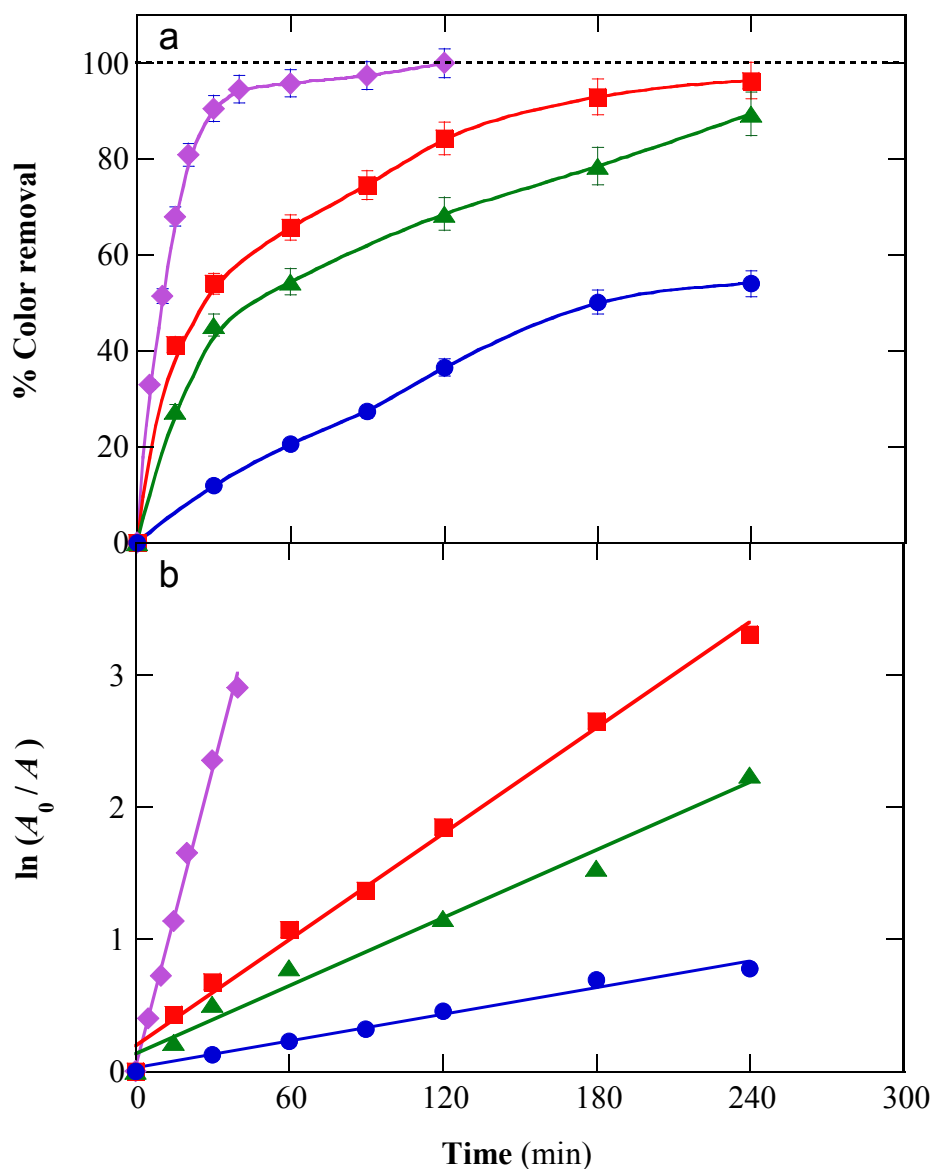
Fig. 5. Influence of pH on (a) the change of percentage of color removal with electrolysis time and (b) the pseudo-first-order kinetics of the absorbance abatement for the AO treatment of 100 mL of 15 mg L^{-1} AB29 in 0.050 M NaCl using a 7YSZ/stainless steel (SS) cell at 10 mA cm^{-2} and 25 ºC. Solution pH: (◆) 3.0, (■) 5.0, (▲) 7.0 and (●) 9.0.

Fig. 6. Percentage of color removal vs. electrolysis time for the AO process of 100 mL of AB29 solutions at pH 7.0 and 25 ºC with a 7YSZ/SS cell. (a) Influence of current density for 15 mg L^{-1} dye in 0.050 M NaCl. (b) Influence of NaCl concentration for 15 mg L^{-1} dye at 10 mA cm^{-2}. (c) Influence of AB29 content for 0.050 M NaCl and 10 mA cm^{-2}.
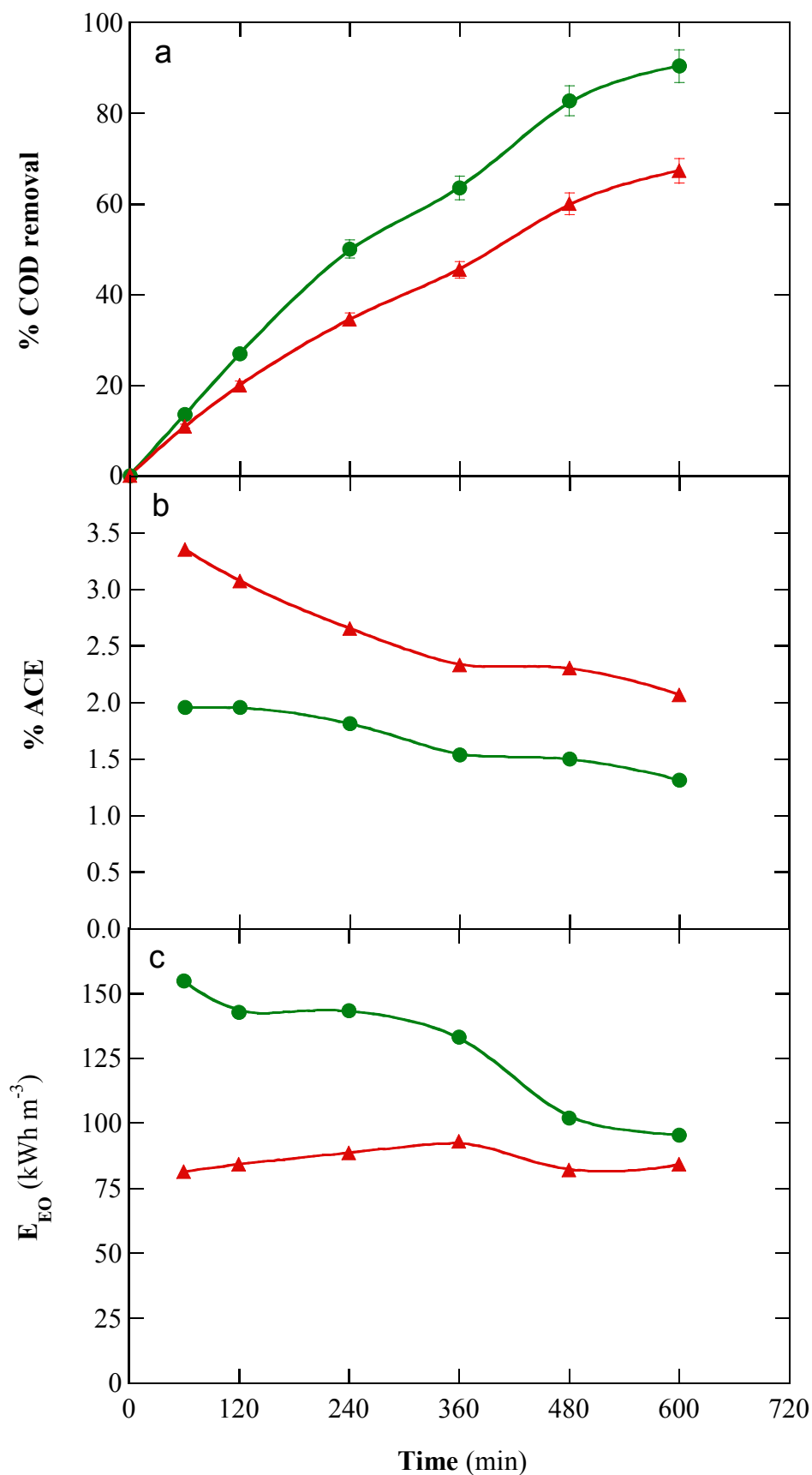
Fig. 7. Variation of (a) percentage of COD, (b) percentage of average current efficiency and (c) electrical energy per order for the AO process of 100 mL of 15 mg L^{-1} AB29 (COD$_0$ = 53.5 mg O$_2$ L^{-1}) in (●) 0.050 M Na$_2$SO$_4$ or (▲) 0.050 M NaCl at pH 7.0 and 25 ºC using a 7YSZ/SS cell. Applied current density: (●) 20 mA cm^{-2} and (▲) 10 mA cm^{-2}.
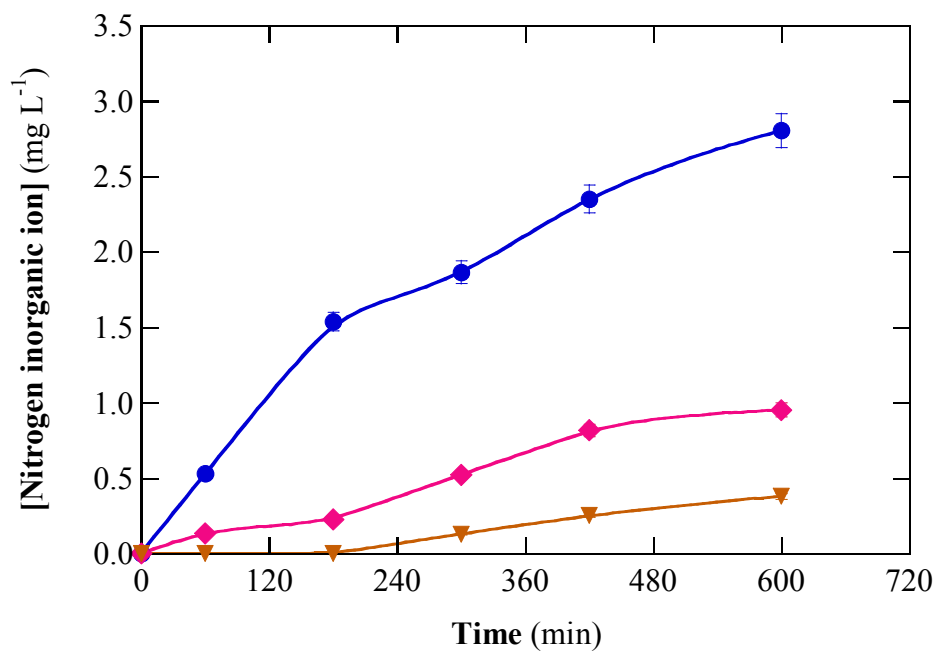
Fig. 8. Time course of the concentration of (●) NO_3^-, (◆) NH_4^+ and (▼) NO_2^- ions released during the AO process of 100 mL of 15 mg L^{-1} AB29 in 0.050 M Na_2SO_4 at pH 7.0 and 25 ºC with a 7YSZ/SS cell at 20 mA cm^{-2}.
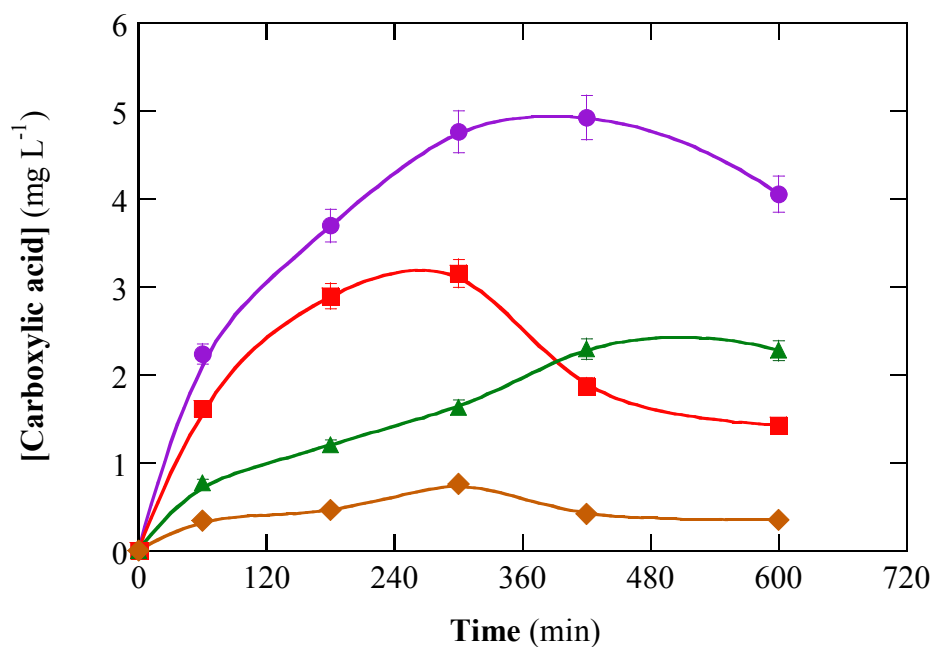
Fig. 9. Change of the concentration of (●) tartaric, (◆) maleic, (■) acetic and (▲) oxalic acids detected during the treatment of 100 mL of 15 mg L^{-1} AB29 in 0.050 M Na_2SO_4 at pH 7.0 and 25 °C by AO using a 7YSZ/SS cell at 20 mA cm^{-2}.

Table 1.

Percentage of color removal at the end of the treatment of 100 mL of AB29 solutions in sulfate (at 360 min) or chloride (at 240 min) media using a 7YSZ/SS cell under selected conditions, as well as the corresponding pseudo-first-order rate constant for decolorization with its squared correlation coefficient.

pH	Current density (mA cm^{-2})	[Electrolyte] (mM)	[AB29] (mg L^{-1})	% color removal	k_{dec} (10^{-3} min^{-1})	R^2
Sulfate medium						
3.0	20	0.050	15	98.9	12.6	0.996
5.0	20	0.050	15	97.0	9.4	0.991
7.0	5	0.050	15	62.2	2.8	0.992
	10	0.050	15	80.0	4.4	0.991
	20	0.025	15	78.7	4.4	0.993
		0.050	10	99.6	10.9	0.997
			15	93.8	7.7	0.997
			30	74.6	3.8	0.990
			60	48.3	1.8	0.990
		0.075	15	93.9	7.8	0.998
		0.100	15	94.6	8.1	0.997
	30	0.050	15	95.2	8.3	0.995
9.0	20	0.050	15	83.7	5.0	0.995
Chloride medium						
3.0	10	0.050	15	100	74.5	0.994
5.0		0.050	15	96.3	13.4	0.992
7.0	5	0.050	15	48.4	2.7	0.980
	10	0.025	15	70.5	4.6	0.980
		0.050	10	95.1	19.9	0.965
			15	89.4	8.6	0.980
			30	76.8	5.9	0.993
			60	59.1	3.7	0.965
		0.075	15	77.0	5.8	0.972
		0.100	15	60.0	3.7	0.993
	20	0.050	15	85.2	7.0	0.976
	30	0.050	15	72.4	3.1	0.970
9.0	10	0.050	15	54.0	3.4	0.983

A ceramic electrode of ZrO$_2$-Y$_2$O$_3$ for the generation of oxidant species in anodic oxidation. Assessment of the treatment of Acid Blue 29 dye in sulfate and chloride media

Alexsandro Jhones dos Santos,[a] Sergi Garcia-Segura,[b] Sergi Dosta,[c] Irene García Cano,[c] Carlos A. Martínez-Huitle,[d] Enric Brillas[a,*]

[a] *Laboratori d'Electroquímica dels Materials i del Medi Ambient, Secció de Química Física, Facultat de Química, Universitat de Barcelona, Martí i Franquès 1-11, 08028 Barcelona, Spain*

[b] *Nanosystems Engineering Research Center for Nanotechnology-Enabled Water Treatment, School of Sustainable Engineering and the Built Environment, Arizona State University, Tempe, AZ 85287-3005, USA*

[c] *CPT Thermal Spray Centre, Materials Engineering, Secció de Ciència de Materials, Facultat de Química, Universitat de Barcelona, Martí i Franquès 1-11, 08028 Barcelona, Spain*
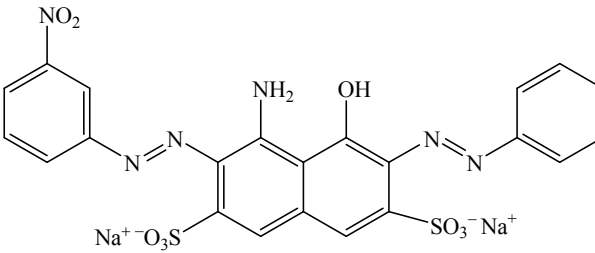
[d] *Laboratório de Eletroquímica Ambiental e Aplicada, Instituto de Química, Universidade Federal do Rio Grande do Norte, Lagoa Nova - CEP 59.072-900, Natal, RN, Brazil*

Corresponding author: * brillas@ub.edu (E. Brillas)

Table S1. Examples over the recent use of ceramic anodes to remove organic pollutants by EAOPs.

Method	Pollutant	Operating conditions	Ceramic anode	Main results	Reference
Anodic oxidation	0.1 mM amoxicillin	230 mL, 50 mM Na_2SO_4, pH 5.7, I: 10-120 mA	Ti_4O_7	69% TOC removal. Better performance compared to DSA and Pt anodes.	[26]
Anodic oxidation	5.0-90 mg L^{-1} Acid Blue 29	100 mL, 50 mM Na_2SO_4, pH = 5, 7, 9, 11, j = 5.0-30 mA cm^{-2}	Sn-Cu-Sb	Complete color and COD removals after 300 and 600 min, respectively, at j = 10 mA cm^{-2}	[28]
Anodic oxidation	100 mg L^{-1} norfloxacin	250 mL, 14 mM Na_2SO_4 j = 33–83 mA cm^{-2}	SnO_2-Sb_2O_3	69% TOC removal after 250 min at j = 83.3 mA cm^{-2}	[29]
Anodic oxidation	100 mg L^{-1} norfloxacin	250 mL, 2 g L^{-1} Na_2SO_4 j = 80 mA cm^{-2}	$(Sn,Sb,Cu)O_2$	84% TOC removal after 240 min. Better performance than SnO_2-Sb_2O_3, but worse than BDD (95% TOC removal)	[30]
Electro-Fenton	0.1 mM amoxicillin	230 mL, 50 mM Na_2SO_4, 0.1 mM Fe^{2+}, pH 3, I: 10-120 mA	Ti_4O_7	Complete degradation in 50 min and 84% TOC removal after 600 min at I = 120 mA	[27]

Table S2. Characteristics of AB29 diazo dye

Chemical structure	
Chemical name	disodium 4-amino-5-hydroxy-3-[(3-nitrophenyl)azo]-6-(phenylazo)naphthalene-2,7-disulfonate
Chemical formula	$C_{22}H_{14}N_6Na_2S_2O_9$
Color Index number	20460
M (g mol^{-1})	616.49
λ_{max} (nm)	600
Visible spectrum	